The Role of Defects on the Assembly and Stability of DNA Nanostructures

*Daniel G. Greene, Jung-Won Keum, and Harry Bermudez**

With a persistence length of 50 nm,[1] double-stranded DNA (dsDNA) is an ideal building material for nanostructures. In addition, because DNA strands hybridize in a well-defined fashion, structures can be built via a "bottom-up" approach. Since the early work of Seeman,[2] many different structures have been created, such as polyhedra, reconfigurable objects, rudimentary computers and walking devices.[3] The development of intricate structures requires unique stabilization methods such as "cross-over" motifs.[4] On the other hand, smaller and simpler structures have potential as drug or gene delivery vehicles.[5–8] Given the small characteristic length of these structures, defects and their locations are expected to play an increasingly important role. However, efforts to date have been largely focused on the roles of flexible spacers (i.e., unpaired bases) during assembly.[9] Here we report that both the assembly and the thermal stability of self-assembled DNA triangles is affected by the density of nick defects. Similar experiments with both newly designed and existing DNA pyramids demonstrated consistent results, suggesting a general behavior for these types of nanostructures. We emphasize that such nick defects, unlike mismatch or gap defects, are unavoidable during the DNA self-assembly process. Furthermore, in contexts where DNA nanostructures must be responsive (e.g., sensors, actuators), noncovalent approaches to affect stability are especially valuable.

Four DNA triangles, designated T1 through T4, served as the starting point for this study. We emphasize that all the triangles have *identical* overall sequence compositions (Tables S1 and S2, Supporting Information (SI)). In other words, the percentage of each nucleobase (i.e., A = adenine, G = guanine, C = cytosine, and T = thymine) is held constant. Each triangle comprises three oligonucleotides, denoted in each case by S1, S2, and S3. In any given triangle, the three strands hybridize to form structures as schematically depicted in **Figure 1**. The strand sequences derive from one face of a previously reported tetrahedron,[5,10] and include unpaired A's, as needed, to provide flexibility at vertices.[11] Each edge of the triangle is designed to be of length $a \approx 7$ nm (i.e., 20 bp). T1 and T3 have nick defects located at each vertex (Figure 1a,c), while T2 and T4 have nick defects located at each edge midpoint (Figure 1b,d). Importantly, triangles T1 and T2 have the same edge sequence compositions (see color-coding in Figure 1). Triangles T3 and T4 also have identical edge sequence compositions, which were obtained by a "rotation" of T1 and T2.

Native polyacrylamide gel electrophoresis (PAGE) was used to demonstrate that the triangle assembly occurs as intended (Figure 1). Interestingly, triangles T2 and T4 show a minor but well-defined larger structure (Figure 1b, d), which is absent in T1 and T3. The appearance of these larger byproducts was our first clue that nick defects could affect assembly, even when keeping sequence composition fixed. Due to the hybridization nature of the self-assembly, linear concatemers are also possible products. The defect density in such concatemers would facilitate their cyclization at lengths far below the persistence length of intact double-stranded DNA.[1] Because of unpaired A's at their vertices, both T2 and T4 have a greater defect density per unit length than T1 and T3. Therefore, T2 and T4 should form cyclization products more readily than T1 and T3. Cyclization products (due to their large size) necessarily require higher concentrations to form than triangular structures, providing a qualitative test for their presence. Assembly experiments performed at lower DNA concentrations, but constant mass, show substantial reduction of larger byproducts (**Figure 2**), consistent with a concentration-dependent cyclization mechanism. Gel analysis reveals that for a twofold reduction in concentration, the triangle yield remains constant within 7%, while the larger products are reduced by 25–35%. As expected, the formation of larger structures comes at the expense of triangle assembly yield (**Table 1**). Similar concentration-dependent effects on DNA nanostructure assembly have been observed and even exploited by others.[3] Structures formed by the cross-assembly of "partial" triangles would be polydisperse and would appear as a smear on the electrophoresis gels, which is not observed to any significant extent. Nevertheless, in all cases the triangles are formed with relatively high efficiency (Table 1).

Dynamic light scattering was performed on gel-purified samples (Figure S1, SI) in order to corroborate DNA triangle assembly. The mean hydrodynamic radii R_h all agree well with each other (Table 1). Curiously, the R_h are about twice as large as expected from the design: the radius of a circle circumscribed

D. G. Greene, J.-W. Keum
Department of Chemical Engineering
University of Massachusetts
Amherst, MA, USA
Prof. H. Bermudez
Department of Polymer Science and Engineering
University of Massachusetts
Amherst, MA, USA
E-mail: bermudez@polysci.umass.edu

DOI: 10.1002/smll.201102221

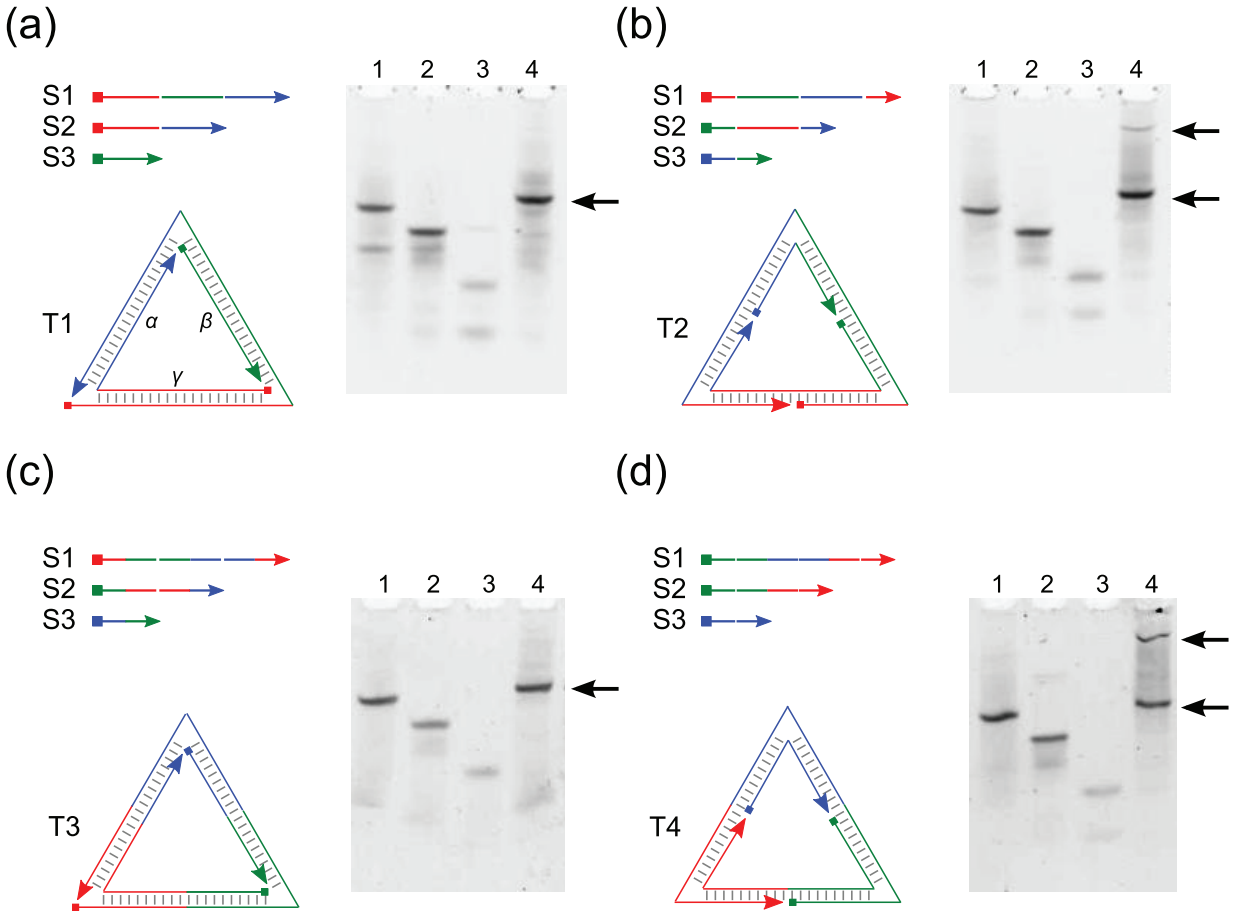

Figure 1. Schematic of the DNA triangles and their assembly. Triangles a) T1, b) T2, c) T3, and d) T4. The colored regions represent identical sequence compositions among all four triangles, and specific edges are denoted by Greek letters. Polyacrylamide gels to the right of each triangle demonstrate the assembly proceeds as intended. In each gel, lane 1: S1+S2; lane 2: S1+S3; lane 3: S2+S3; lane 4: S1+S2+S3 (all). The arrows are meant to indicate the desired structures and a larger by-product.

about the triangles is $(\sqrt{3}/3)a \approx 4$ nm. This effect has been observed in other DNA nanostructure size analysis,[12] and we speculate that it could be due to a convolution from the desired structures and larger by-products. It is well known that even small amounts of a larger by-product will cause strong scattering. In the future, more extensive measurements at various scattering angles,[13] may be able to resolve this issue. While not definitive, the DLS data in conjunction with the electrophoresis data strongly suggest that the structures were correctly assembled. Furthermore, the melting experiments conducted (see below) are consistent with triangle assembly.

By using the intercalating dye SyBr Green, the thermal stability of these DNA structures could be assessed. This dye is strongly fluorescent in the presence of double-stranded DNA; by monitoring the fluorescence F over a range of temperatures, thermal transitions can be identified. We note that while label-free methods can also be used to determine thermal transitions, fluorescence presents two major advantages over

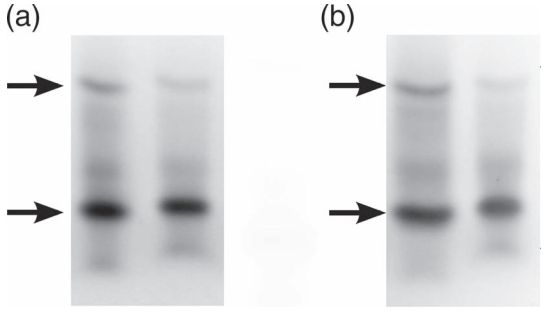

Figure 2. Concentration-dependent formation of assembly byproducts determined by polyacrylamide gel analysis of triangles a) T2 and b) T4. The black arrows are meant to indicate the desired structures and the larger cyclization byproduct. In each gel, lane 1: 0.30 μM and lane 2: 0.15 μM, with the total mass held constant.

Table 1. DNA triangle characteristics: assembly yield, mean hydrodynamic radius R_h, and maximum melting temperature T_m^*.

Sample	Yield [%]	R_h [nm]	T_m^* [°C]
T1	87[a)]	10.4 ± 1.5	68[b)]
T2	85[a)]	8.8 ± 1.1	62
T3	82	7.8 ± 1.3	66
T4	78	7.7 ± 1.0	61

[a)]Mean ±2.5% based on triplicate experiments; [b)]taken as the highest-temperature peak location.

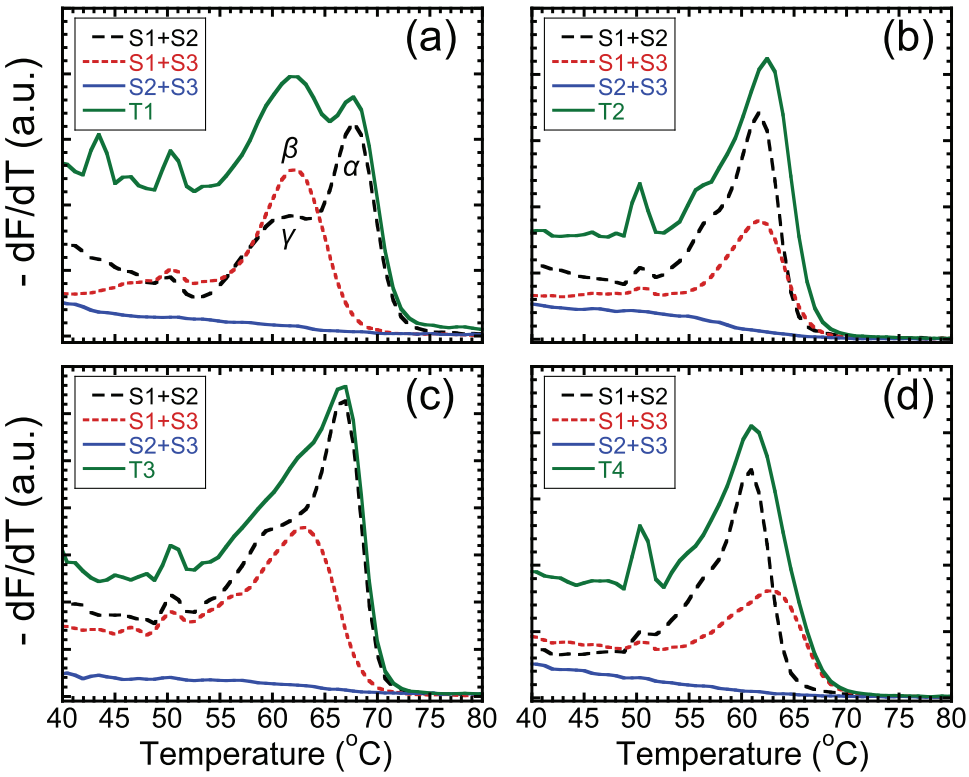

Figure 3. Real-time fluorescence to determine the thermal transitions of DNA triangles and their corresponding 2-strand complexes, labeled with presumed edge contributions. a) T1, b) T2, c) T3, and d) T4.

UV–vis spectroscopy and circular dichroism: i) the dynamic range is linear over a wider concentration range and ii) the signal-to-noise ratio is higher.[14] Irrespective of the method, the thermal transitions are most readily visualized by plotting $-dF/dT$ versus T, generating a so-called melting curve. Using the SyBr Green dye, melting curves were obtained for each triangle and its 2-strand complexes (**Figure 3**), with minimal effects due the presence of the dye (Table S3, SI). In all cases the triangles have peaks corresponding to the superposition of their respective 2-strand complexes. Such superposition can be understood if each triangle segment melts independently of the others,[11] and would be consistent with defects serving as nucleation sites for the melting process. While this explanation is tentative, there is substantial experimental[15–18] and modeling[19,20] evidence supporting such a view of melting in *linear* dsDNA. In the context of a DNA nanostructure, the defect density sets a length scale, which we refer to as the "melt length" l_m. By inspection of Figure 1, T1 and T3 have l_m = 20 bp, whereas T2 and T4 have l_m = 10 bp.

It is intuitively expected that as the defect density ($\sim 1/l_m$) increases, the maximum melting temperature T_m^* would decrease, and indeed, the data show that T1 and T3 are more thermally stable than their counterparts T2 and T4 (Table 1 and Figure 3). Calculation of melting temperatures using the *NUPACK* software[21] gave general agreement with the experimentally measured trends, further supporting that dye effects are minimal. However, the calculated T_m values did not correctly reflect differences between triangles and their rotated analogues (e.g., T1 versus T3), highlighting the fact that the observed behavior is not solely of thermodynamic origin.

Because the overall sequence composition is held constant, it becomes apparent that the edge composition is responsible for the particular features of each triangle. For example, the melting of triangle T1 displays a bimodal character (Figure 3a). If we examine the 2-strand complexes of T1, we see that since strands S1+S3 form only one edge (labeled β in Figure 1a), it has a single peak that defines a single melt temperature $T_{m,\beta}$. On the other hand, hybridization of strands S1+S2 results in two edges (labeled α and γ in Figure 1b). The difference in *edge* sequence composition is large enough to result in a bimodal curve: a shoulder and a peak at a higher temperature (Figure 3a). We rationalize that the shoulder is the result of two factors: first, edge γ is 45% G/C, which is nearly the same in composition as edge β (50% G/C) (Table S2, SI). This compositional similarity is likely to explain why $T_{m,\gamma} \approx T_{m,\beta}$. Second, edge γ contains a stretch of five contiguous A/T's adjacent to a vertex (see Table S1, SI). Such weaker base-pairing would facilitate melting and counteract the appearance of a well-defined peak. The observation that $T_{m,\gamma} < T_{m,\alpha}$ appears to be a result of edge α having a relatively high G/C content of 65%. To verify that the results of Figure 3a were not due to a lack of T1 assembly, the appropriate band was purified by gel-extraction prior to the melting experiment. The resulting melting curve is bimodal, just as that of the crude T1 (Figure S2, SI).

Triangle T2 has a defect at each edge midpoint *and* an unpaired A at each vertex, and therefore its melt length l_m is 10 bp (Figure 1b). When comparing T2 against T1, we find that T2 is less thermally stable than T1: $T_m^{*,T2} < T_m^{*,T1}$ (Table 1), strengthening the notion of a correlation between

NANO MICRO small

l_m and T_m^*. We presume that T2 and its 2-strand complexes share the same l_m (Figure 3b) because all have the same l_m and all have similar G/C contents along their edges. Triangles T3 and T4 both show a single broad peak (Figure 3c,d). Just as for T2, these broad peaks presumably arise because the melting peaks of their 2-strand complexes are distinct yet sufficiently close to each other. When comparing T4 against T3, we find that T4 is less thermally stable than T3: $T_{m,T4}^* < T_{m\,T3}^*$ (Table 1), which is again consistent with differences in l_m.

In comparing triangles with the same l_m (i.e., T1 versus T3 or T2 versus T4), the positions of intermediate peaks are shifted by the edge composition. Indeed, these composition differences suggest an explanation for an interesting feature of T4: in that triangle, T_m for S1+S2 < T_m for S1+S3. Although the l_m are equal for these complexes, the edge composition is substantially lower in G/C content for S1+S2 than S1+S3. Furthermore, a stretch of five A/T's is adjacent to the nick defect in S1+S2 (Figure 1d), weakening this location. A simpler argument based on the overall hybridization length of T4's 2-strand complexes would incorrectly predict that T_m for S1+S3 < T_m for S1+S2. While overall hybridization length could be used to explain the melt curves for T1 and T3, it cannot explain the data for T2 and T4.

Although not definitive without many additional experiments, the assembly and stability results support an interpretation based primarily on differences in l_m, rather than on differences in edge composition. To improve the thermal stability of T2 and T4, their l_m could in principle be increased by enzymatically ligating the edge midpoint nicks. However, due to the increased rigidity of DNA at the lengths used here (≈10 nm), the efficiency of ligases is questionable.[16,22] Indeed, we have previously reported reduced nuclease activity when the substrates are a group of related DNA triangular pyramids.[5] While chemical ligation provides an alternative to enzymatic methods, we note that the biological activity of nucleic acid can be adversely affected by such covalent presentation.[23] Especially in contexts where DNA nanostructures must be responsive (e.g., sensors,[24] delivery vehicles[6]), noncovalent methods to improve stability, such as defect placement, provide an attractive strategy.

We recognize that many different combinations of nick defect locations (and hence l_m) could be explored, and the l_m would not necessarily be constant across different regions of a given structure. It must be therefore considered if an (arithmetic) average melt length $\langle l_m \rangle$ is meaningful. The melt length is related to the defect density, which in turn affects the nucleation and progression of melting. Because nucleation is a local process, and because we observe superposition of melt profiles (Figure 3), we conclude that a simple average quantity such as $\langle l_m \rangle$ is of limited usefulness. Indeed, preliminary experiments with *asymmetric* nick defect distributions indicate a more complex picture than the results presented here (data not shown). Given the vast number of potential defect combinations, further work on the effects of defects in DNA nanostructures will most likely require the assistance of computational modeling.

As a further test of the picture outlined so far, we examined the role of nick defects using a series of four triangular pyramids. We have included in this group a previously reported pyramid,[10] denoted here as P1 (**Figure 4**a), as well as its "nick-rotated" analogue P2 (Figure 4b). We

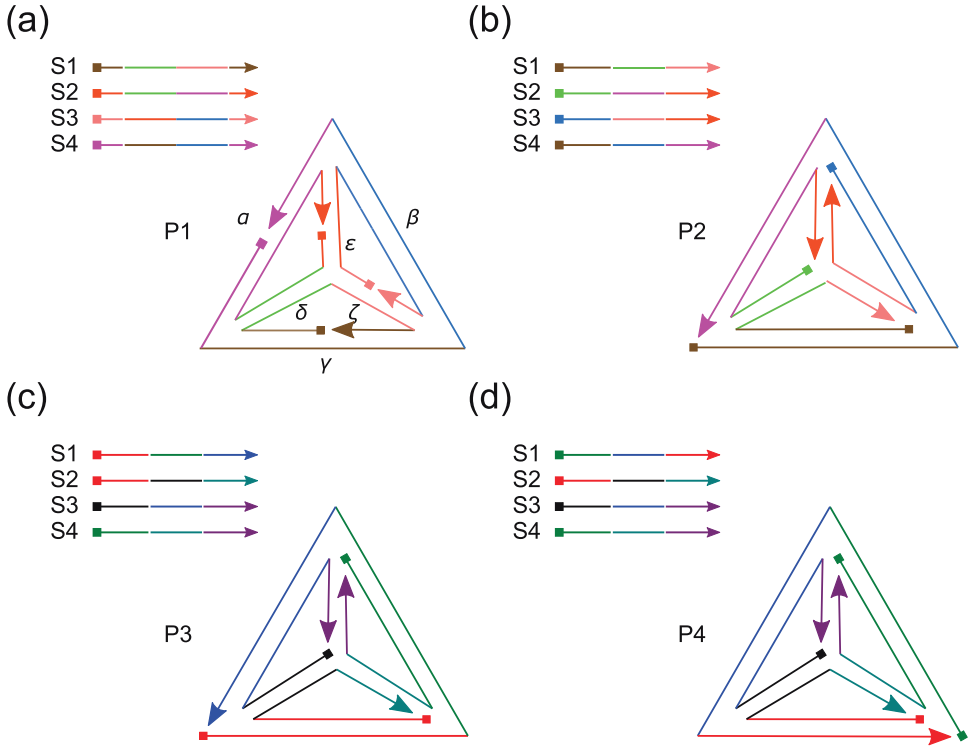

Figure 4. Schematic two-dimensional projection of DNA pyramids. a) A previously reported DNA pyramid,[10] denoted here as P1, and b) its "nick-rotated" analogue P2. Two newly designed pyramids c) P3 and d) its analogue P4. The colored regions represent identical sequence compositions among each pair of pyramids, and specific edges are denoted by Greek letters.

also used the Tiamat software,[25] to design pyramids P3 and P4 (Figure 4c,d), such that they are identical to each other in sequence composition, have an edge length $a \approx 7$ nm, but have different nick defect locations. That the assembly proceeds as intended is demonstrated by native PAGE (Figure S3, SI). Pyramid P1 has an asymmetric defect distribution (i.e., l_m is not constant): four of the six edges in P1 have midpoint defects and correspond to $l_m = 10$ bp. As mentioned earlier, because melt lengths cannot be simply averaged, we tentatively consider P1 as a pyramid with $l_m \approx 10$ bp. By contrast, pyramids P2, P3, and P4 have a constant $l_m = 20$ bp throughout their entire structures.

Consistent with the triangle experiments, the melting curves for pyramids and their 3-strand complexes also reveal superposition (Figure S4, SI). Several comparisons can be made from pyramid melting curves (**Figure 5**), which give additional insight into the role of defects on thermal stability. Most importantly, for two pyramids with identical sequence composition, the l_m is significantly lower for P1 than for P2 (Figure 5a), supporting the role of l_m established with simpler 2D triangles. We note that the magnitude of the difference in peak melting temperatures (≈6 °C) is similar to that for the triangles (Table 1), although additional experiments would be needed to decouple specific sequence composition effects. Another fairly straightforward comparison is that of P2 and P3, two pyramids which have identical l_m but different sequence compositions. The lower G/C content of P2 (Table S2, SI) presumably leads to $T_m^*{}_{,P2} < T_m^*{}_{,P3}$.

The comparison of P3 and P4 is a special case because although the l_m and sequence composition are identical, P4 has a vertex with *two* defects (Figure 4d). The identical l_m peaks for these pyramids (Figure 5b), is a striking result that strongly supports the role of l_m. The absence of a lower l_m peak in P4, as compared to P3, is due to a combination of factors. First, the vertex defined by the intersection of edges γ, β, and ζ in both P3 and P4 (Figure 4c,d) is intrinsically weakened by a locally high A/T content (Table S1, SI). In P3, the hybridization interactions near this weak vertex are adequate to give rise to the lower l_m peak, whereas in P4 the increased defect density is sufficiently destabilizing to abolish the corresponding peak. The common l_m value for P3 and P4 primarily arises from a *single* 3-strand intermediate (S1+S3+S4) (Figure S4, SI), that is responsible for the three edges with the highest G/C contents (Table S2, SI).

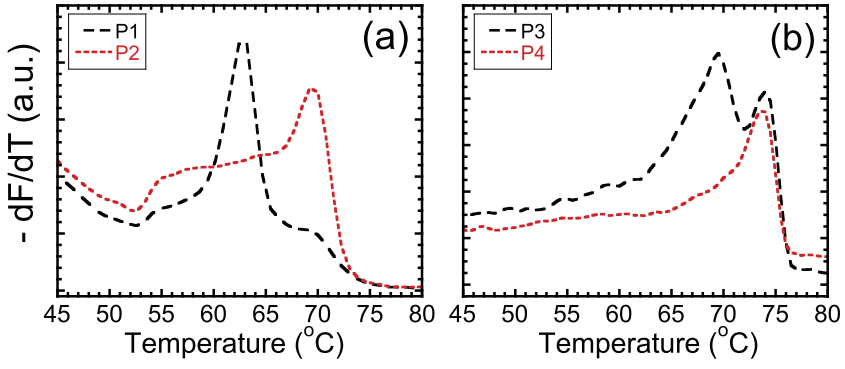

Figure 5. Real-time fluorescence to determine the thermal transitions of DNA pyramids a) P1, P2, and b) P3, P4.

We have shown that defect density has a significant impact on both the assembly and thermal stability of simple DNA nanostructures. The local sequence composition of the nanostructures typically manifests itself when adjacent to a defect site, in agreement with the composition-dependent weakening near defects found in short linear dsDNA.[26] In applications such as drug and gene delivery, it is recognized that stability and responsiveness must be balanced. Defects complement chemical approaches to tune the responsiveness of DNA nanostructures, in particular with respect to external stresses. Such stresses could arise at the molecular scale: ATP-driven motors (ATP = adenosine triphosphate) and DNA-binding proteins, or at the bulk scale: fluid shear and osmotic pressure.[27] The deliberate introduction of locally weak regions within DNA nanostructures provides an innate mechanism for release of encapsulants, in contrast to many strategies which rely on additional DNA strands as external triggers.[28] We note that the concept of using "failure" as a design element has precedents in both natural and man-made contexts: for example, seed dispersal and automobile crumple zones.

Experimental Section

Assembly and Electrophoresis: All oligonucleotides were purchased from Integrated DNA Technologies. A programmable thermal cycler (Bio-Rad iCycler) was used for all assembly and disassembly experiments. To assemble the triangles, component strands were mixed in equimolar amounts to a final total concentration of 0.3 μM. Triangles were hybridized in TM buffer (10 mM Tris, 5 mM $MgCl_2$). The strands were heated to 95 °C and held there for 10 min, followed by cooling at a rate of 0.5 °C s^{-1} to 4 °C where they were held for at least 10 min before use. To assemble pyramids, stoichiometric quantities of the component DNA strands were mixed in TM buffer to a final total concentration of 0.5 μM. Solutions were heated at 95 °C for 10 min, followed by step-wise cooling of 60 °C for 1 h, 30 °C for 1 h and finally to 4 °C.

Hybridization between component DNA strands was analyzed with 8% and 5% native poly-acrylamide gels for triangles and pyramids, respectively. The assembly yields of triangles presented in Table 1 of the manuscript were obtained by measuring band intensities of triangles with ImageJ, and normalizing with respect to the appropriate S1+S2 band (see Figure 1). Briefly, since the gel staining dye (Gelstar, Lonza) signal is proportional to the mass of double-stranded DNA, the expected ratio of 3-strand structures (i.e., triangles) to 2-strand structures is 3:2. The fractional deviations from the above ratio are taken as the assembly yield, recognizing that this approach underestimates the true yield.

Purification: Samples were purified using Freeze-n-Squeeze kit (Bio-Rad). First, a polyacrylamide gel was loaded with hybridized sample and run at 70 V for 1 h to resolve individual bands. The gel was then washed with TM buffer to remove the running buffer (towards mimicking conditions during synthesis and melting). Individual bands were then cut out

NANO MICRO small

of the gel and loaded onto the Freeze-n-Squeeze column. The column was placed at −20 °C for 8 min. After freezing, it was spun at 16 000*g* for 3 min. The flowthrough was diluted with TM buffer (to 420 μL) and was subsequently passed through a 0.22 μm filter into a low-volume cuvette.

Dynamic Light Scattering (DLS): DLS measurements were made on purified samples (see SI) using a Malvern Zeta Sizer Nano-ZS. The wavelength of the laser was 632.8 nm, the scattering angle was 173°, and the temperature was 25 °C. Analysis was performed using the CONTIN method. The distributions are shown in Figure S1 (SI) and summarized in Table 1 of the manuscript.

Fluorescence Monitoring of Melting: Samples were prepared in a similar fashion to the assembly and thus the samples are in TM buffer. SyBr Green purchased from Bio-Rad was added to the samples to achieve a final concentration of 0.1–0.5×. The samples were then melted using the heating block of a Bio-Rad iCycler from 20 to 95 °C at increments of 0.5 °C. The samples dwelled at each temperature for 10 s and the iCycler camera measured the fluorescence at each dwell. The derivative of the fluorescence with respect to temperature was numerically calculated using the iCycler software.

Supporting Information

Supporting Information is available from the Wiley Online Library or from the author.

Acknowledgements

The authors thank B. Sidhom for initial pyramid experiments and the NSF (DMR-0847558) for financial support.

[1] a) D. Shore, J. Langowski, R. L. Baldwin, *Proc. Natl. Acad. Sci. USA* **1981**, *78*, 4833–4837; b) J. Bednar, P. Furrer, V. Katritch, A. Z. Stasiak, J. Dubochet, A. Stasiak, *J. Mol. Biol.* **1995**, *254*, 579–94; c) J. P. Peters, L. J. Q. Maher, *Rev. Biophys.* **2010**, *43*, 23–63.

[2] a) N. C. Seeman, N. R. Kallenbach, *Biophys. J.* **1983**, *44*, 201–209; b) N. C. Seeman, *J. Biomol. Struct. Dyn.* **1990**, *8*, 573–581.

[3] a) Y. He, T. Ye, M. Su, C. Zhang, A. E. Ribbe, W. Jiang, C. Mao, *Nature* **2008**, *452*, 198–201; b) U. Feldkamp, C. M. Niemeyer, *Angew. Chem., Int. Ed.* **2006**, *45*, 1856–1876; c) N. C. Seeman, *Trends Biochem. Sci.* **2005**, *30*, 119–25; d) J.-W. Keum, A. P. Hathorne, H. Bermudez, *Wiley Interdiscip. Rev. Nanomed. Nanobiotechnol.* **2011**, *3*, 282–97.

[4] a) J. H. Chen, M. E. Churchill, T. D. Tullius, N. R. Kallenbach, N. C. Seeman, *Biochemistry* **1988**, *27*, 6032–6038; b) T. J. Fu, N. C. Seeman, *Biochemistry* **1993**, *32*, 3211–20; c) X. J. Li, X. P. Yang, J. Qi, N. C. Seeman, *J. Am. Chem. Soc.* **1996**, *118*, 6131–6140.

[5] J.-W. Keum, H. Bermudez, *Chem. Commun.* **2009**, 7036–7038.

[6] J.-W. Keum, J.-H. Ahn, H. Bermudez, *Small* **2011**, *7*, 3529–3535.

[7] C. M. Erben, R. P. Goodman, A. J. Turberfield, *Angew. Chem., Int. Ed.* **2006**, *45*, 7414–7417.

[8] B. P. Duckworth, Y. Chen, J. W. Wollack, Y. Sham, J. D. Mueller, T. A. Taton, M. D. Distefano, *Angew. Chem., Int. Ed.* **2007**, *46*, 8819–8822.

[9] a) Y. He, C. D. Mao, *Chem. Commun.* **2006**, 968–969; b) C. L. P. Oliveira, S. Juul, H. L. Jørgensen, B. Knudsen, D. Tordrup, F. Oteri, M. Falconi, J. Koch, A. Desideri, J. S. Pedersen, F. F. Andersen, B. R. Knudsen, *ACS Nano* **2010**, *4*, 1367–76.

[10] R. P. Goodman, I. A. T. Schaap, C. F. Tardin, C. M. Erben, R. M. Berry, C. F. Schmidt, A. J. Turberfield, *Science* **2005**, *310*, 1661–1665.

[11] J. L. Kadrmas, A. J. Ravin, N. B. Leontis, *Nucleic Acids Res.* **1995**, *23*, 2212–2222.

[12] C. Zhang, M. Su, Y. He, Y. Leng, A. E. Ribbe, G. Wang, W. Jiang, C. Mao, *Chem. Commun.* **2010**, *46*, 6792–6794.

[13] F. B. Bombelli, F. Gambinossi, M. Lagi, D. Berti, G. Caminati, T. Brown, F. Sciortino, B. Norden, P. Baglioni, *J. Phys. Chem. B* **2008**, *112*, 15283–15294.

[14] B. Sacca, R. Meyer, C. M. Niemeyer, *Nat. Protoc.* **2009**, *4*, 271–285.

[15] M. D. Frank-Kamenetskii, Y. S. Lazurkin, *Annu. Rev. Biophys. Bioeng.* **1974**, *3*, 127–150.

[16] D. A. Erie, R. A. Jones, W. K. Olson, N. K. Sinha, K. J. Breslauer, *Biochemistry* **1989**, *28*, 268–273.

[17] I. A. Il'icheva, D. Y. Nechipurenko, S. L. Grokhovsky, *J. Biomol. Struct. Dyn.* **2009**, *27*, 391–8.

[18] Y. Zeng, A. Montrichok, G. Zocchi, *J. Mol. Biol.* **2004**, *339*, 67–75.

[19] Y. Kafri, D. Mukamel, L. Peliti, *Eur. Phys. J. B* **2002**, *27*, 135–146.

[20] a) E. J. Sambriski, D. C. Schwartz, J. de Pablo, *Proc. Natl. Acad. Sci. USA* **2009**, *106*, 18125–30; b) E. J. Sambriski, V. Ortiz, J. J. de Pablo, *J. Phys.: Condens. Matter* **2009**, *21*, 034105.

[21] J. N. Zadeh, C. D. Steenberg, J. S. Bois, B. R. Wolfe, M. B. Pierce, A. R. Khan, R. M. Dirks, N. A. Pierce, *J. Comput. Chem.* **2011**, *32*, 170–3.

[22] M. E. Hogan, M. W. Roberson, R. H. Austin, *Proc. Natl. Acad. Sci. USA* **1989**, *86*, 9273–9277.

[23] X. Tang, M. Su, L. Yu, C. Lv, J. Wang, Z. Li, *Nucleic Acids Res.* **2010**, *38*, 3848–55.

[24] W. Wang, Y. Yang, E. Cheng, M. Zhao, H. Meng, D. Liu, D. Zhou, *Chem. Commun.* **2009**, 824–826.

[25] S. Williams, K. Lund, C. Lin, P. Wonka, S. Lindsay, H. Yan, In *DNA computing: 14th international meeting on DNA computing* (Eds: A. Goel, F. C. Simmel, P. Sosik), 1st ed., Springer, New York, **2009**; Vol. *5347*, pp 90–101.

[26] E. Protozanova, P. Yakovchuk, M. D. Frank-Kamenetskii, *J. Mol. Biol.* **2004**, *342*, 775–85.

[27] a) V. A. Parsegian, R. P. Rand, D. C. Rau, *Proc. Natl. Acad. Sci. USA* **2000**, *97*, 3987–92; b) P. L. Hansen, R. Podgornik, V. A. Parsegian, *Phys. Rev. E* **2001**, *64*, 021907.

[28] a) R. P. Goodman, M. Heilemannt, S. Dooset, C. M. Erben, A. N. Kapanidis, A. J. Turberfield, *Nat. Nanotechnol.* **2008**, *3*, 93–96; b) Z. Wu, H. Zhou, S. Zhang, X. Zhang, G. Shen, R. Yu, *Chem. Commun.* **2010**, *46*, 2232–2234.

Received: October 20, 2011
Revised: December 13, 2011
Published online: February 22, 2012

